Nano Energy 96 (2022) 107105

Contents lists available at ScienceDirect

Nano Energy

journal homepage: www.elsevier.com/locate/nanoen

Hydrogen bonds enhanced composite polymer electrolyte for high-voltage cathode of solid-state lithium battery

Yongtao Wang [a,b,1], Lingqiao Wu [a,b,1], Zhiyuan Lin [a,b], Mingxue Tang [c], Peipei Ding [a,b], Xianwei Guo [a,b,*], Zihe Zhang [a,b], Shiqi Liu [a,b], Boya Wang [a,b], Xin Yin [a,b], Zonghai Chen [d], Khalil Amine [d,**], Haijun Yu [a,b,*]

[a] Institute of Advanced Battery Materials and Devices, Faculty of Materials and Manufacturing, Beijing University of Technology, Beijing 100124, PR China
[b] Key Laboratory of Advanced Functional Materials, Ministry of Education, Beijing University of Technology, Beijing 100124, PR China
[c] Center for High Pressure Science & Technology Advanced Research, Beijing 100094, PR China
[d] Chemical Sciences and Engineering Division, Argonne National Laboratory, 9700, South Cass Avenue, Lemont, IL 60439, United States

ARTICLE INFO

Keywords:
Composite solid electrolyte
Hydrogen bonds
Electrochemical stability window
High-voltage cathode
Solid-state lithium batteries

ABSTRACT

Polymer electrolyte is one of the important components for developing advanced solid-state lithium batteries (SSLBs). However, the narrow electrochemical stability window restricts the practical application with high-voltage cathodes. Herein, a series of composite solid electrolytes (CSEs), possessing both wide electrochemical stability window (up to 5.0 V vs. Li^+/Li) and high ionic conductivity (over 1.35 $\times 10^{-3}$ S/cm at 25 °C), were reported by integrating SiO_2 nanoparticles into poly(vinyl ethylene carbonate) polymer electrolyte. The enhanced anti-oxidation performances are mainly caused and confirmed by the local intermolecular interactions of hydrogen bonds in CSE. Based on this CSE, the SSLBs with $LiCoO_2$ cathode present good cycle stability at high voltage, and the capacity retention with 4.5 V cut-off voltage is about 94% after 200 cycles. This work not only proves the importance of intermolecular interactions in CSE, but also provides an effective method for achieving high-energy SSLBs with enhanced interface compatibility between polymer electrolyte and high-voltage cathodes.

1. Introduction

The rechargeable lithium ion batteries (LIBs) are widely used in portable electronic devices and electric vehicles, and their energy densities can be further promoted by applying the high-voltage and high-capacity cathode materials [1–7]. However, the development of high-energy LIBs is still suffered from the security issue of fire and explosion during the utilization of liquid electrolyte [8]. In order to improve the safety and stability, the solid-state lithium batteries (SSLBs) have been extensively studied, in which the solid-state electrolyte (SSE) is one of the important components [9–11]. Compared to the inorganic oxide and sulfide electrolytes [12,13], the polymer electrolytes (PEs), possessing the high flexibility, light weight, and excellent processing, are considered as the preferable choice for large-scale applications [14]. More importantly, the PEs play the basic role for assembling SSLBs, the ions conducting and anti-oxidation abilities have greatly influences on electrochemical performances. Nevertheless, the ionic conductivities of PEs are always lower than those of commercial liquid electrolytes ($\geq 10^{-3}$ S/cm at room temperature, 25 °C) [13–15]. Even worse, the narrow electrochemical stability window of PEs has restricted their practical applications with high-voltage cathode materials for high-energy SSLBs.

To address these problems, various PEs have been designed, such as the poly(propylene carbonate) (PPC) [15], poly(vinylene carbonate acrylonitrile) (P(VCA-AN)) [16], diethylene glycol-fluorinated triethylene glycol (DEG-FTriEG) [17], poly(methyl hydrosiloxane) (PMHS) [18], and P(STFSILi)-PEO-P(STFSILi) [19]. However, the ionic conductivities of these PEs are still below than 10^{-3} S/cm at 25 °C, although the relatively wide electrochemical stability window can be available in some systems [17,19,20]. Recently, the poly(vinyl ethylene

* Corresponding authors at: Institute of Advanced Battery Materials and Devices, Faculty of Materials and Manufacturing, Beijing University of Technology, Beijing 100124, PR China.
** Corresponding author.
E-mail addresses: xwguo@bjut.edu.cn (X. Guo), amine@anl.gov (K. Amine), hj-yu@bjut.edu.cn (H. Yu).
[1] Both authors contributed equally to this paper.

https://doi.org/10.1016/j.nanoen.2022.107105
Received 16 January 2022; Received in revised form 22 February 2022; Accepted 27 February 2022
Available online 28 February 2022

carbonate) polymer electrolyte (PVEC-PE) with superior conductivity of 2.1×10^{-3} S/cm at 25 °C has been reported for SSLBs [21]. However, the anti-oxidation ability of PVEC-PE is still not enough for high-voltage cathode materials with charge potential of 4.5 V (vs. Li^+/Li). The organic-inorganic composite solid electrolytes (CSEs), in which the inorganic fillers and polymer matrix can be combined together, are one of the effective methods to improve the anti-oxidation ability of PEs [22–24]. In the past, a variety of CSEs have been reported, such as polytetrafluoroethylene-$Li_{6.75}La_3Zr_{1.75}Ta_{0.25}O_{12}$-Succinonitrile (PTFE-LLZTO-SN) [25], LLZTO-PEO [26], LLZO-PEO [27], PVDF-LLZTO [28], PAN-LLZTO [29], PAN-LAGP [30] and PEO/PEG-$Li_{10}GeP_2S_{12}$ [31]. However, the relative mechanisms for the enhanced performance are still not clear in the CSEs. Although the Lewis acid-base interactions are proposed to explain the reason for wide electrochemical stability window in PEO/$LiClO_4$-Al_2O_3 [32], Ca-CeO_2/LiTFSI/PEO [33] and PEO-$LiZr_2(PO_4)_3$ [34], the evidences for the existence of interactions are still lacking. Even more, the ionic conductivities of these CSEs are still not comparable with that of liquid electrolyte at 25 °C.

Herein, based on our previous work [21], a series of CSEs have been reported, which possess wide electrochemical stability window and high ionic conductivity. Both the effect of local intermolecular interactions on the anti-oxidation ability and lithium ions migration mechanism in the CSE have been revealed by theoretical calculations and experimental results. Furthermore, based on these CSEs, the electrochemical performances of high-voltage cathode material with charge potential of 4.5 V (vs. Li^+/Li) have also been explored, providing an effective way for improving the cycle stability of SSLBs with high energy density.

2. Experimental section

2.1. Fabrication of composite solid electrolyte (CSE) and solid-state battery

The CSEs with tunable size was fabricated by the solution-casting method [21]. Firstly, liquid VEC monomer (~72–76 wt%) and bistrifluoromethanesulfonimide lithium (LiTFSI) (~23 wt%) were added into the glass bottle under stirring to form a homogeneous solution in a glove box. Subsequently, different contents of hydrophilic silica (~1–5 wt%) and 2,2′-Azobis(2-methylpropionitrile) (AIBN) (~1 wt%) as the catalyst were added into the solution and stirred for 12 h. Then the homogeneous mixed solution was poured into the Whatman® filter (100% borosilicate glass fiber) (~140–160 μm) on the PTFE plate, followed by the polymerization in a vacuum oven at 80 °C for 12 h.

For the fabrication of the solid-state battery based on the composite solid electrolyte via in-situ polymerization process, the details are as follows. Typically, the mixed solution with 10 μl was injected into the cathode and 20 μl was injected to Whatman® filter in coin-type battery (CR2032), which was adopted as support for composite solid electrolyte, and separator between cathode and anode to prevent the internal short circuit of the battery before polymerization. After that, the battery was assembled and transferred to a vacuum oven at 80 °C for 12 h to make the complete polymerization.

2.2. Structural characterizations

The Fourier Transform Infrared Spectroscopy (FT-IR) was carried out using a Nexus 870 FTIR spectrometer instrument to distinguish the structures of liquid VEC monomer and CSE. The crystal structure of the CSE was characterized via XRD with a range of 10°-80°. The morphology and thickness of the CSE was characterized by a field emission scanning electron microscope (SEM, Hitachi S-4800). TG ((Netzsch 449F3) was carried out to measure the thermal property of the composite solid electrolyte from 25 to 600 °C at a heating rate of 10 °C/min under nitrogen atmosphere. Raman spectra were recorded on a confocal Raman microscope (WITec, German) with an excitation wavelength of 532 nm.

Solid-state Nuclear Magnetic Resonance (ssNMR) spectra of ^6Li, ^7Li and ^1H were acquired from a Bruker Avance III 400 spectrometer. The samples were finely packed into 4 mm zirconia rotors in the glove box. All spectra were recorded after single-pulse excitation. The NMR spectral simulations were done by Dimfit 2015 software.

The bulk resistance of composite solid electrolytes was tested by Electrochemical Impedance Spectroscopy (EIS) using Solartron 1470E cell test system at varied temperatures, and the ionic conductivity was calculated from equation: $\sigma = L/R_bS$, where R_b is the bulk resistance, L and S are the thickness and area of the composite solid electrolyte, respectively. The electrochemical stability window was investigated by linear sweep voltammetry (LSV) performed on a working electrode of SS (SS: stainless steel), Li metal as the counter and reference electrode at a scan rate of 1.0 mV/s between 2 and 5.5 V. The lithium-ion transference number (t_{Li}^+) was calculated by the chronoamperometry test on the Li/CSE/Li symmetry battery with an applied voltage of 0.01 V and was determined by following equation: $t_{Li}^+ = \frac{I_{ss}(V-I_0R_0)}{I_0(V-I_{ss}R_{ss})}$, where I_0 and I_{ss} are the initial and steady-state currents, and R_0 and R_{ss} are the first and last resistances, respectively. The tests were completed by EIS measurements taken before and after the polarization scans over a frequency range of 0.1–10^6 Hz with a 10 mV amplitude at 25 °C. The temperature-dependent ionic conductivity behavior of CSEs can be fitted by the Arrhenius plots as equation $\sigma = AT^{1/2}\exp\left[\frac{-E_a}{R(T-T_0)}\right]$, where A is the pre-exponential factor, E_a is the activation energy, and T is the absolute temperature, T_0 is the Vogel scaling temperature at which the free volume disappears or at which configuration free entropy becomes zero (T_0 = 236/K), and *R* is the ideal gas constant.

2.3. Theoretical simulation

All the density functional theory (DFT) calculations were carried out by using Gaussian software [35]. Geometric configurations were optimized at the B3LYP-D3 level with a 6–311 + G (d, p) basis set [36–39]. The 6–311 +G(d, p) basis set is a split-valence triple-zeta basis with diffuse s and p functions for non hydrogen atoms. Such basis set has good accuracy, and widely used in previous works [40–42]. The vibrational frequency calculations were performed at the same computational level to confirm that the configurations were energetic minima.

2.4. Battery characterization

The composite cathode for solid-state battery was composed of 80 wt% $LiCoO_2$ (LCO) cathode material, 10 wt% carbon black, 10 wt% binder. The battery with LCO areal density of ~2.5 mg/cm^2 has been explored. The solid lithium metal batteries composed of both LCO cathode that assembled by the in-situ process were charged and discharged between 3.0 and 4.6 V at varied current densities. The C rates in all the electrochemical measurements are defined based on 1 C = 160 mA /g for LCO. The battery was assembled in an argon-filled glove box, with oxygen and H_2O content less than 0.1 ppm. The galvanostatic charge/discharge tests of CR2032 were conducted on LAND testing system (Wuhan LAND electronics Co., Ltd.) at 25 °C. For comparison, the batteries were assembled and tested with commercial liquid carbonate electrolyte (1.0 M $LiPF_6$ in a mixture of ethylene carbonate and dimethyl carbonate (1:1 by volume) and liquid VEC electrolyte (LiTFSI-VEC without polymerization) at 3.0–4.6 V. To examine the cathodes after battery measurement, the batteries were firstly disassembled in an Ar filled glove box.

3. Results and discussions

3.1. Fabrication and characterizations of CSE

The CSE membrane was prepared by the “solvent-free” solution casting method [21] (Fig. 1a). The SiO_2 nanoparticles (~20–30 nm,

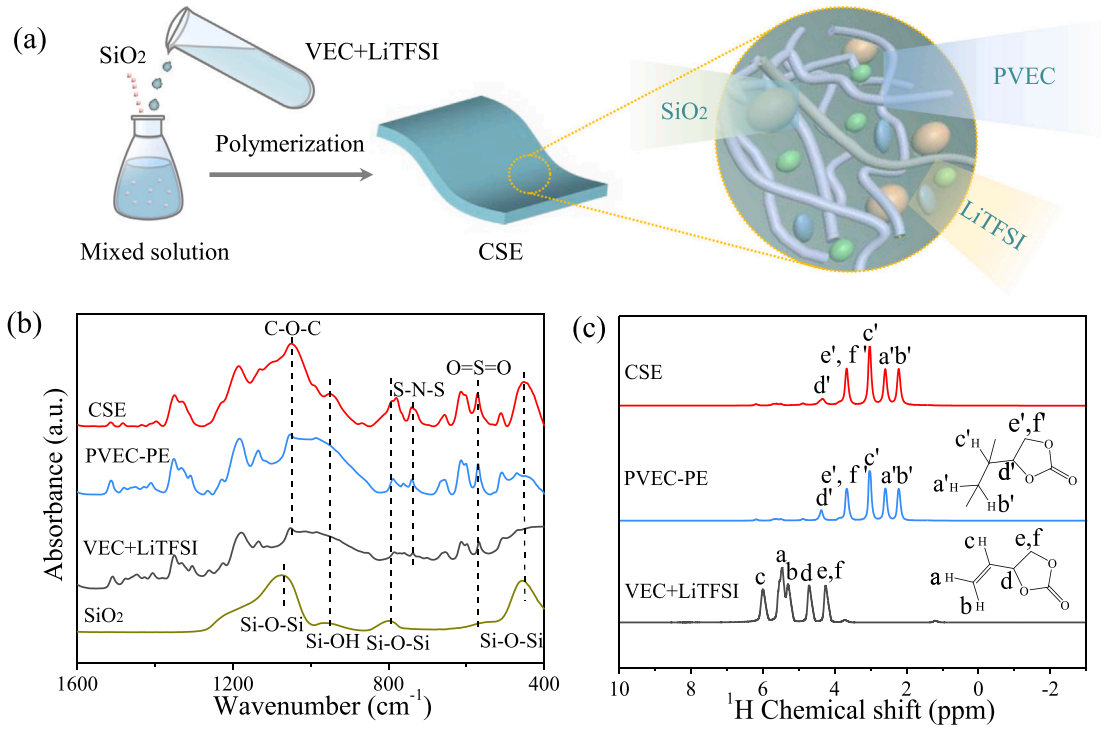

Fig. 1. (a) Schematic diagram of preparing the CSE membrane from VEC precursor with Li salt and nanoparticles. The comparisons of (b) FT-IR and (c) ^{1}H NMR spectra of CSE, PVEC-PE, and VEC+LiTFSI.

Fig. S1) and lithium salt are dispersed uniformly in the VEC liquid precursor, and then the high homogeneity of flexible CSE can be obtained after the polymerization. The microstructure of CSE and relative components have been characterized by Fourier Transform Infrared Spectroscopy (FT-IR) and solid-state Nuclear Magnetic Resonance (ssNMR). Fig. 1b shows the FT-IR spectra of SiO_2, VEC+LiTFSI salt, PVEC-PE and CSE. The peaks at ~571 cm^{-1} and ~745 cm^{-1} are assigned to the asymmetric stretches of O═S═O and S-N-S groups in Li salt (LiTFSI), respectively [43–45]. And the peaks at ~1050 cm^{-1} can be attributed to stretching of C-O-C group in VEC, PVEC-PE and CSE [21, 46,47]. Moreover, the characteristic peaks can be found for both SiO_2 and CSE, in which the peak at ~950 cm^{-1} is assigned to the bending vibrations of Si-OH group, and ~450, ~796 and ~1080 cm^{-1} are identified as the symmetric and antisymmetric vibrations of Si-O-Si group [48]. These typical peaks have confirmed the homogeneous dispersion of nanoparticles in the CSE.

The polymerization reaction from VEC precursor was further verified by ssNMR spectroscopy. The resonance signals shift from downfield to upfield via polymerization process (Fig. 1c), from which the C═C bonds converted to C-C bonds. Particularly, the chemical shifts of 5–6 ppm for VEC+LiTFSI (the H atom at a, b and c position of -CH═CH_2 group) have moved to 2–3 ppm (a′, b′ and c′) for PVEC-PE and CSE, which should be attributed to the formation of -CH-CH_2- after polymerization [46]. These position variances confirm the C═C addition polymerization of VEC monomer in PVEC-PE and CSE. Small amount of residual signals at 4.5–6 ppm is attributed to the unreacted C═C group, which is not possible to be eliminated due to the structural configuration. Thus, the integration of SiO_2 nanoparticles does not affect obviously on the ^{1}H signal when comparing with that of PVEC-PE and CSE. Additionally, the chemical shifts of 4–5 ppm (d, e and f) for the five-membered ring structure have migrated to 3.5–4.5 ppm (d′, e′ and f′), which are caused by the change of chemical environment after polymerization and the local intermolecular interactions (will be discussed later). Protons at e and f positions are almost identical in chemical environments with the same resonance shift. And the weaker signal of protons at e, f (e′, f′) and d′ positions are possibly related to the fast relaxation that caused by the neighboring O atoms and the rigid polymer chains [49,50]. Furthermore, the dense structure of CSE membrane and uniform distribution of nanoparticles are revealed by cross-sectional SEM and EDS mappings (Fig. S2a-b). These properties are favorable for forming fast ion transport channels, and improving the mechanical properties to effectively prevent the inner short-circuit and enhance the safety of batteries. In addition, from the X-ray diffraction (XRD) patterns in Fig. S2c, the CSE membrane shows the low crystallinity structure, which could be beneficial for the fast Li^{+} transports. Moreover, as compared in the thermogravimetric analysis (TGA) of PVEC-PE and CSE, the thermal stability is also increased with the integration of SiO_2 nanoparticles (Fig. S2d).

3.2. *Electrochemical properties of CSE*

The ions conducting ability of solid electrolyte has the critical role for electrochemical performances of SSLBs. Therefore, the ionic conductivities of various CSE-x ($x = 1$~5) with different content of SiO_2 nanoparticles (1~5 wt%) and PVEC-PE have been evaluated over a wide temperature range. As shown in Fig. 2a and S3, the ionic conductivity of CSE-x increases simultaneously when increasing the temperature. Importantly, all the ionic conductivity of CSE-x can still maintain the level of 10^{-3} S/cm at 25 °C. The ionic conductivity and corresponding activation energy of CSE-x has been compared systematically in Fig. 2b. Although the content of nanoparticles increases from 0 to 5 wt%, the ionic conductivity slightly decreases from ~2.1 × 10^{-3} S/cm of PVEC-PE to ~1.35 × 10^{-3} S/cm of CSE-5 at 25 °C. Even more, the activation energy only increases from 0.16 eV to 0.18 eV, which are representing the low energy barrier for Li ions migrations. The ionic conductivity of CSE-6 (the content of SiO_2 nanoparticles is 6 wt%) decreased obviously at 25 °C, so the comprehensive performances of CSE-x ($x \leq 5$) have been systematically explored.

The effect of SiO_2 nanoparticles on the properties of CSEs has been further explored by Li ions transference number (t_{Li}^{+}), which is the mole ratio of mobile cations to that of the total ions (cations and anions) in solid electrolyte [51]. From the direct current polarization and corresponding EIS test, the t_{Li}^{+} increases from 0.40 for PVEC-PE to 0.55 of

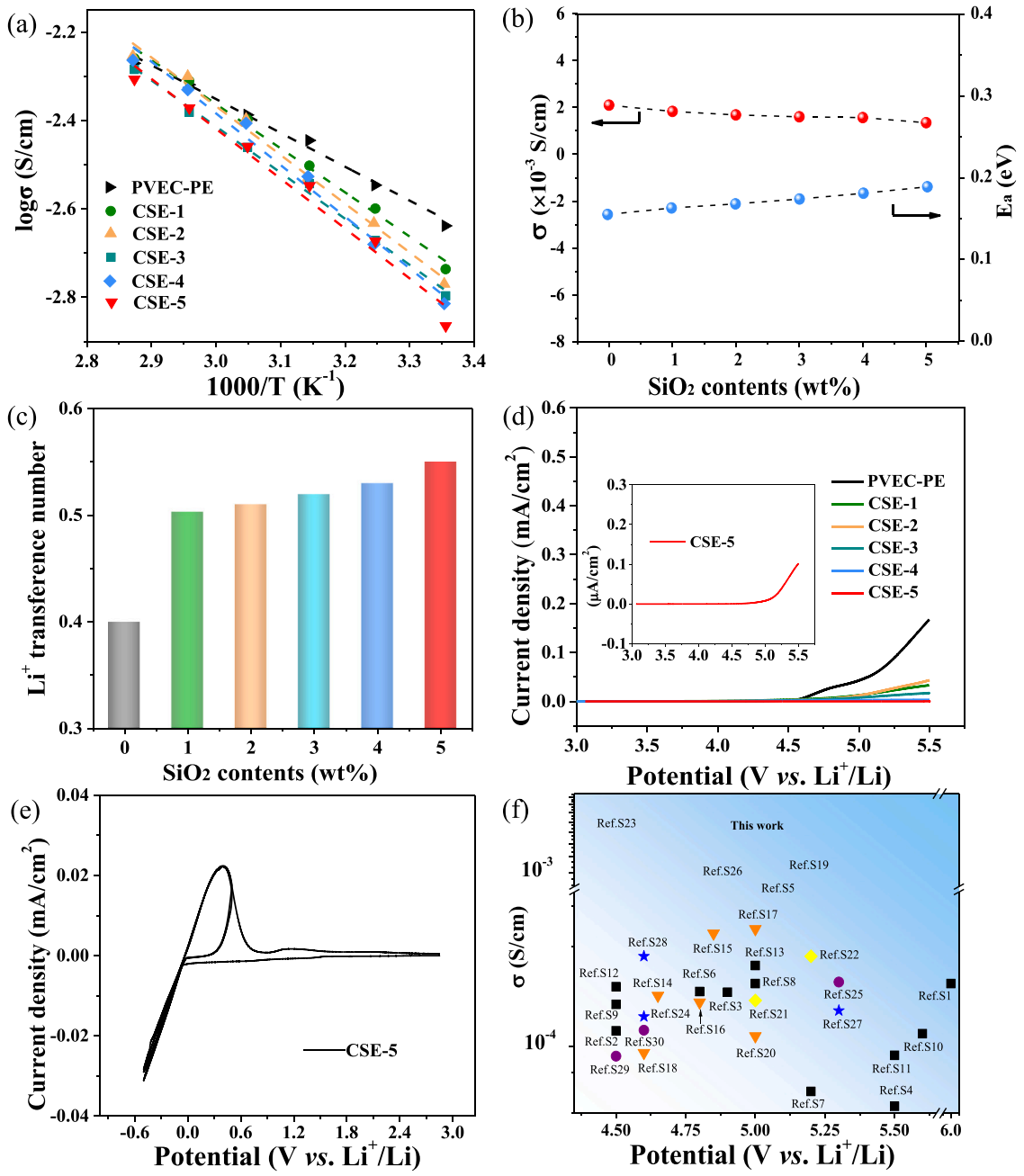

Fig. 2. Properties of CSEs. The comparisons of (a) Arrhenius plots of PVEC-PE and CSEs with different SiO_2 contents, (b) the ionic conductivity and activation energy of CSEs with different content of SiO_2 nanoparticles, (c) the Li ions transference number, (d) the electrochemical stability window. (e) CV curve of Li/CSE-5/SS battery in a voltage range of − 0.5–3.0 V. and (f) The ionic conductivities vs. electrochemical stability window for various solid electrolytes at 25 °C or 30 °C. Note: ■ PEO based, ▼ PVDF based, ◆ PAN based, ★ Carbonate-based, ● Others. More details are provided in Table S1.

CSE-*x* when increasing the content of nanoparticles (Fig. 2c and S4). With the high t_{Li}^+, the ratio of mobile Li ions in CSEs can be increased, and the movement of anions is restrained, which can reduce the concentration polarization and improve the electrochemical performance of SSLBs [52,53]. Moreover, as the increase of t_{Li}^+ in CSE-*x*, plenty of anions are fixed inside of the electrolyte, and then the oxidized decomposition of CSE at high charge voltage can be effectively suppressed [54,55].

Besides the ionic conductivity and t_{Li}^+, the anti-oxidation ability of CSE is also one of the crucial parameters for practical application in high-energy SSLBs. Thus, the variety of electrochemical stability window for CSE-*x* has been detected by LSV of Li/CSE/SS cell. As can be seen in Fig. 2d, the electrochemical stability window of CSE significantly expands to ~5.0 V (vs. Li^+/Li) with 5wt% SiO_2 nanoparticles, which is much higher than that of PVEC-PE. That is, the anti-oxidation ability of polymer electrolyte can be effectively enhanced by integrating low amount of SiO_2 nanoparticles, and it is beneficial for making interface compatibility between polymer electrolyte and high-voltage cathode materials. In addition, the interfacial stability between CSE and Li metal anode was investigated by both Cyclic Voltammetry (CV) and polarization test of the SSLBs. From the CV curve of Li/CSE-5/SS battery in a voltage range of − 0.5–3.0 V (Fig. 2e), there are two peaks at − 0.5 V and 0.5 V for the reversible lithium plating/stripping in different cycles, indicating the electrochemical stability of interface contact between CSE-5 and Li anode. As shown in Fig. S5, the Li/CSE/Li battery shows the low voltage polarization without short circuiting for long cycling

time of 800 h, demonstrating the good reversibility for lithium plating/stripping in SSLBs. Moreover, considering the anti-oxidation and ions conducting abilities, the comprehensive properties of CSE-5 have been compared with those of various PEs and composite electrolytes (Fig. 2f). Obviously, the CSE-5 has the wide electrochemical stability window up to ~5.0 V (vs. Li^+/Li) and high ionic conductivity of ~1.35×10^{-3} S/cm at 25 °C, possessing good comprehensive electrochemical performance and are much better than those of the reported solid electrolytes at the same testing temperature. Thus, the CSE-5 can be applied with high-voltage cathode materials to achieve the high energy density and excellent electrochemical performances of SSLBs.

3.3. The characterizations of local intermolecular interactions in CSE

The origins for the enhanced anti-oxidation ability and increased t_{Li}^+ in CSE-5 has been explored by multiple characterizations. Firstly, the ^{1}H NMR spectra of CSE and PVEC-PE are further analyzed (Fig. 3a). The signal at ~4.4 ppm in PVEC-PE has widen and moved to ~4.35 ppm in CSE-5. And a new chemical shift with relatively high proportion is observed at ~4.45 ppm, which should be attributed to the formation of hydrogen bonds after incorporating SiO_2 nanoparticles [56]. Additionally, compared to the weak peak of ~3580 cm^{-1} in FT-IR for O-H stretching band of PVEC-PE, an obvious and wide peak appears at ~3539 cm^{-1} in CSE-5 (Fig. 3b). The change of peak should be ascribed to the hydrogen bonds between a plenty of H atoms from SiO_2 nanoparticles and O atoms in PVEC molecular skeleton. Moreover, the hydrogen bonds cause the increase of bond length and decrease of bond energy, resulting in the redshift of characteristic peaks [56–58]. Thus, the formation of hydrogen bonds between SiO_2 nanoparticles and polymer chain in the CSE has been confirmed by the ^{1}H NMR and FT-IR.

Furthermore, there are two peaks positioned at ~1789 cm^{-1} and ~571 cm^{-1} of FT-IR (Fig. 3c-d), which are assigned to the stretching vibration of C═O group in polymer chain and asymmetrical stretching of O═S═O group for LiTFSI in PVEC-PE [56]. In the CSE-5, these two peaks have moved to ~1776 cm^{-1} and ~568 cm^{-1} respectively. The redshifts are mainly caused by the increase of bonds length after the formation of hydrogen bonds between SiO_2 and PVEC as well as anions ($TFSI^-$) in Li salt. In the newly formed hydrogen bonds, the donors are H atoms from -OH groups on the surface of SiO_2 nanoparticles, and the acceptors are O atoms from PVEC chain and O═S═O groups of $TFSI^-$. Besides, the formation of hydrogen bonds in CSE-5 has been revealed by Density Functional Theory (DFT) calculations. The electrostatic potentials (ESPs) show the electric density maps of different groups in PVEC and $TFSI^-$ (Fig. 3e). The regions around O atoms on C═O group in PVEC and O═S═O group of $TFSI^-$ have higher electron density, indicating the hydrogen bonds can preferentially form at the O position of these groups in CSE-5. As shown in Fig. 3f, the local intermolecular interactions of hydrogen bonds can form via the H atoms on the surface of SiO_2 and O atoms on the C═O and O═S═O groups in PVEC and $TFSI^-$, respectively. The theoretical calculations are consistent with the experimental results, which have confirmed the local intermolecular interactions in the solid electrolyte.

Moreover, the ion pairing of $TFSI^-$ in CSE-5 has been analyzed by FT-IR and Raman spectroscopy through exploring the bonding between anions of Li salt and H atoms of SiO_2 nanoparticles. The peak centered around 740 cm^{-1} represents the S-N-S stretching vibration of free $TFSI^-$ anions, and it is sensitive to ion pairing [23,34,43]. This peak is dissociated into two peaks at ~738 and ~742 cm^{-1}, which correspond to the free anions and fixed anions respectively (Fig. 3g) [59,60]. After the Gaussian-Lorentzian fitting, the area ratio of fixed anions increases from 33.2% in PVEC-PE to 69.3% in CSE-5, demonstrating that most of the free ion pairs are anchored on the surface of nanoparticles by hydrogen bonds. Then the high t_{Li}^+ can be obtained in CSE-5. The change of content for ion pairs has also been verified by Raman shift of S-N-S group in $TFSI^-$ (Fig. S6). Therefore, the formation of hydrogen bonds among components in CSE-5 has been confirmed by experimental results and

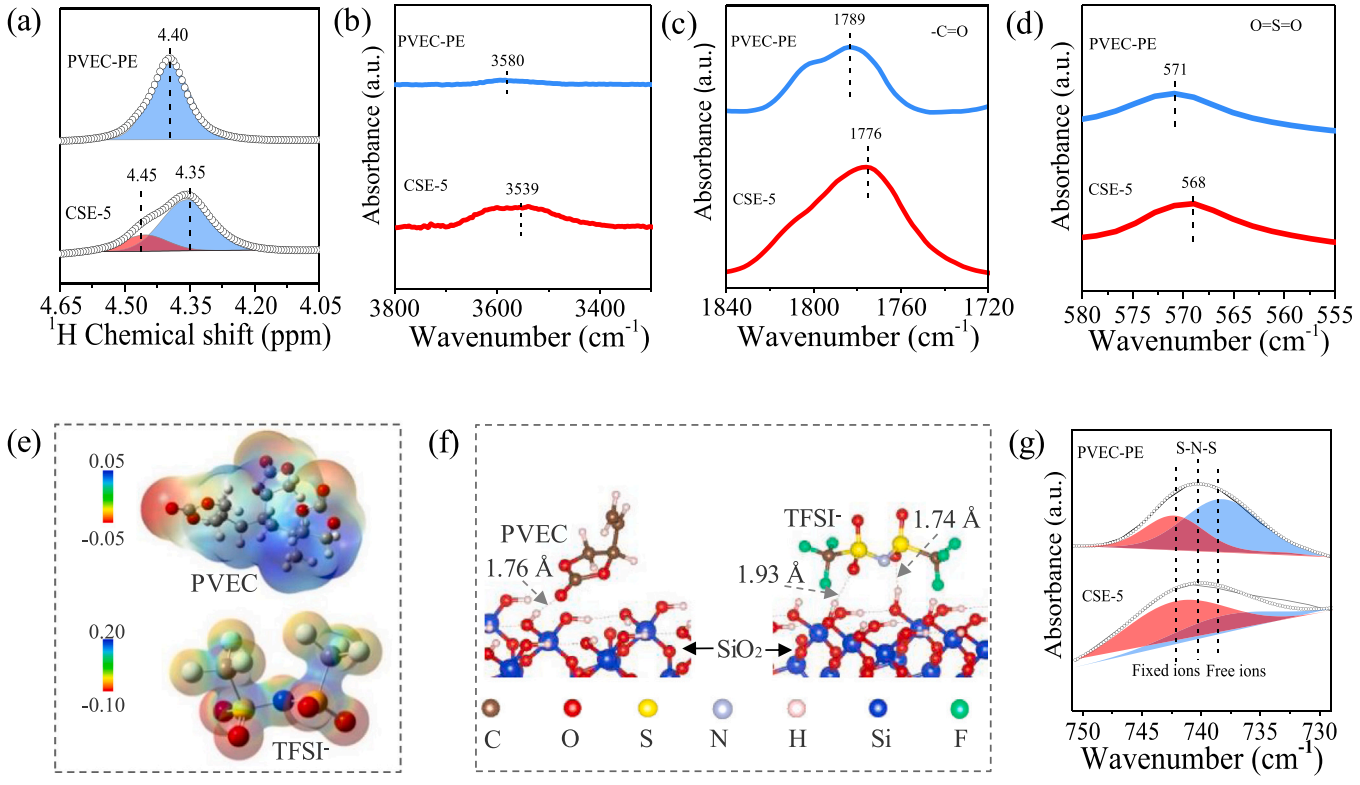

Fig. 3. (a) ^{1}H NMR spectra of PVEC-PE and CSE-5. (b-d) FT-IR spectra of PVEC-PE and CSE-5. (e) Molecular electrostatic potential energy mappings of PVEC and $TFSI^-$. (f) Intermolecular interaction in CSE by DFT calculation. (g) FT-IR spectra of PVEC and CSE-5 at 740 cm^{-1}.

theoretical calculations, and these local intermolecular interactions are responsible for enhancing the anti-oxidation ability and increasing the t_{Li}^{+} of polymer electrolyte.

3.4. Mechanism of Li^{+} transports in CSE

The high ionic conductivity of CSE should be closely related to the ions migration pathways, which is determined by both PVEC-PE matrix and SiO_2 nanoparticles with local intermolecular interactions. Here the ions migration mechanism in CSE-5 has been investigated by ssNMR. The Li/CSE-5/Li symmetric battery was assembled and cycled for different time, and the interactions between cations and functional groups are analyzed by both ^{7}Li and ^{6}Li NMR spectra [61,62]. As shown in Fig. 4a, the pristine electrolyte shows one ^{7}Li NMR signal at ~0.2 ppm, which shifts to 0 ppm upon cycling. It has the same tendency as that of PVEC-PE, and should be attributed to the interaction between the mobile Li ions and O atoms of C═O groups in polymer chains [21]. Furthermore, the relaxation time (T_1) increases from ~0.29 s to ~0.42 s with increased cycle time, indicating the enhancement of Li ions mobilities, and the structure of functional group was activated and loosened during ions migration. Due to smaller quadrupole moment of ^{6}Li, the well-resolved ^{6}Li NMR spectra of the same electrolytes are also performed. As shown in Fig. 4b, the same shift trend is observed for ^{6}Li when compared to ^{7}Li NMR spectra, which demonstrates the strong interaction between Li ions and C═O groups for different time (signals at ~0 ppm). However, the intensity ratio of this interaction decreases with long cycle time. Meanwhile, a new chemical shift of ~− 0.1 ppm can be observed, and is representing the interaction between Li ions and O atoms in C-O groups. Furthermore, after the simulations of these interactions for different cycle time, the intensity ratio of Li ions attached to C═O groups (0 ppm) decreases from ~79% to ~54%, while intensity ratio of Li ions localized to C-O group (−0.1 ppm) increases from ~21% to ~35%. These tendencies of ssNMR in CSE-5 are similar to that of PVEC-PE, indicating the fast ions migrations were mainly achieved by the interactions between Li ions and O atoms of C═O/C-O groups [21].

In addition, there is another new signal at ~0.2 ppm can be probed in CSE-5. As the local intermolecular interactions of hydrogen bonds have formed in CSE-5, this chemical shift should be attributed to the ions migration along the interface between SiO_2 nanoparticles and PVEC-PE. With long time, the intensity ratio of interface ions migration in CSE-5 becomes more obvious. The interface ions migration has also been reported in other CSEs [61–64]. The different ions migration pathways and relative proportion with various cycle time has been compared in Fig. 4c. Obviously, for the main ions migration pathways that achieved by the interaction with C═O and C-O groups, the proportion of the former decreases with the increasing time, while the proportion of the later increases subsequently. Moreover, the proportion of interface ions migration in CSE-5 has increased, which is caused by the local intermolecular interactions. Thus, the ^{6,7}Li NMR results reveal the relocating of Li ions, which is strongly correlating with the ionic migration behaviors. Compared with PVEC-PE, the decrease of ionic conductivity for CES-5 should be attributed to the decrease of interaction between Li ions and C═O groups. However, as the increase of interaction between Li ions and C-O groups, and the appearance of interface ions migration, the ionic conductivity of CSE-5 still keeps the level of 10^{-3} S/cm at 25 °C. Accordingly, the mixed ions migration mechanism in CSE-5 is exhibited in Fig. 4d. With the host material of PVEC-PE, the fast and dominant Li ions migration can be achieved by interactions with O atoms of C═O groups (Path 1). And the migrations could be proceeded through the interactions with O atoms of C-O groups (Path 2). Besides, the Li ions

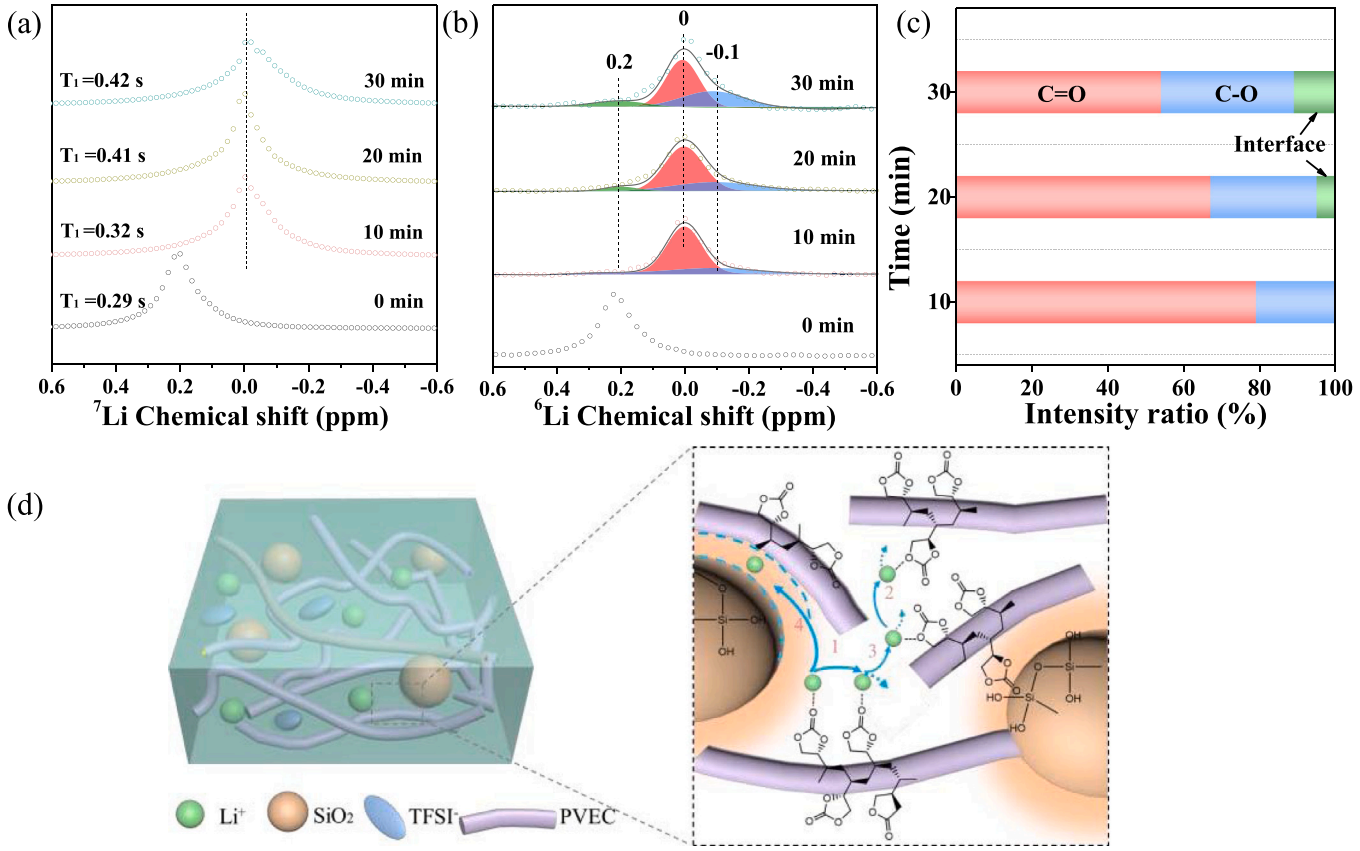

Fig. 4. (a) ^{7}Li and (b) ^{6}Li NMR spectra of CSE after different cycle time (T_1 is the relaxation time). The open circles are experimental signals and the dark lines in (b) are the sum of simulations. (c) The main ions transport pathways and relative proportions with various cycle time in CSE. (d) Schematic diagram of the Li ions transport pathways in the CSE.

migrations by the moving/exchange between C-O and C═O groups is also existing (Path 3). More importantly, with the local intermolecular interaction of hydrogen bonds, the interface ions migration (Path 4) plays an important role for the high ionic conductivity of composite electrolyte.

3.5. Electrochemical performances of CSE based SSLBs

With the wide electrochemical stability window and high ionic conductivity at 25 °C, the CSE-5 has been applied for $LiCoO_2$ (LCO) cathode materials with high charge voltages. The solid-state LCO/CSE-5/Li battery was assembled in one step via in-situ polymerization of electrolyte precursor. The EDS mappings show the uniform distribution of elements in composite cathode (Fig. S7), demonstrating the sufficient permeation of CSE-5 to provide enough ions conductive pathways. Fig. 5a shows that the LCO/CSE-5/Li battery can be charged steady to 4.6 V under 0.1 C at 25 °C, however, LCO/PVEC-PE/Li battery could not be applied in the same situation. It has confirmed that the anti-oxidation ability of PVEC-PE can be enhanced after the combination of nanoparticles. As shown in Fig. S8, the LCO cathode with commercial liquid carbonate electrolyte displays the typical charge-discharge profiles with high capacity in 3.0–4.6 V. However, with the VEC+LiTFSI electrolyte, the LCO cathode cannot charged to 4.4 V at the first charge process. Furthermore, as shown in Fig. 5b and S9a, the LCO/CSE-5/Li battery exhibits the galvanostatic charge/discharge curves with the initial discharge capacity of ~175 mA h/g, indicating the practical application of CSE for high energy SSLBs with high-voltage cathode materials. However, as the high catalytic effect of cobalt oxide at high charge potential, the CSE-5 was oxidized and easily to be decomposed [65]. Besides, the structure of LCO material is extremely unstable after repeated charging/discharging at this charge potential [66,67]. Thus, the cycling stability of solid-state LCO/CSE-5/Li battery is not satisfactory when the cathode material is charged to 4.6 V.

In order to enhance the lifetime, the solid-state LCO/CSE-5/Li battery was evaluated in the voltage range of 3.0–4.5 V at 25 °C. As shown in Fig. 5c, the LCO/CSE-5/Li battery shows the initial discharge capacity of ~153 mA h/g and initial Coulombic efficiency of ~75%. The LCO/PVEC-PE/Li battery displays a similar discharge capacity, but the overpotential between charge and discharge potentials is much higher than that of LCO/CSE-5/Li battery. The low overpotential of LCO/CSE-

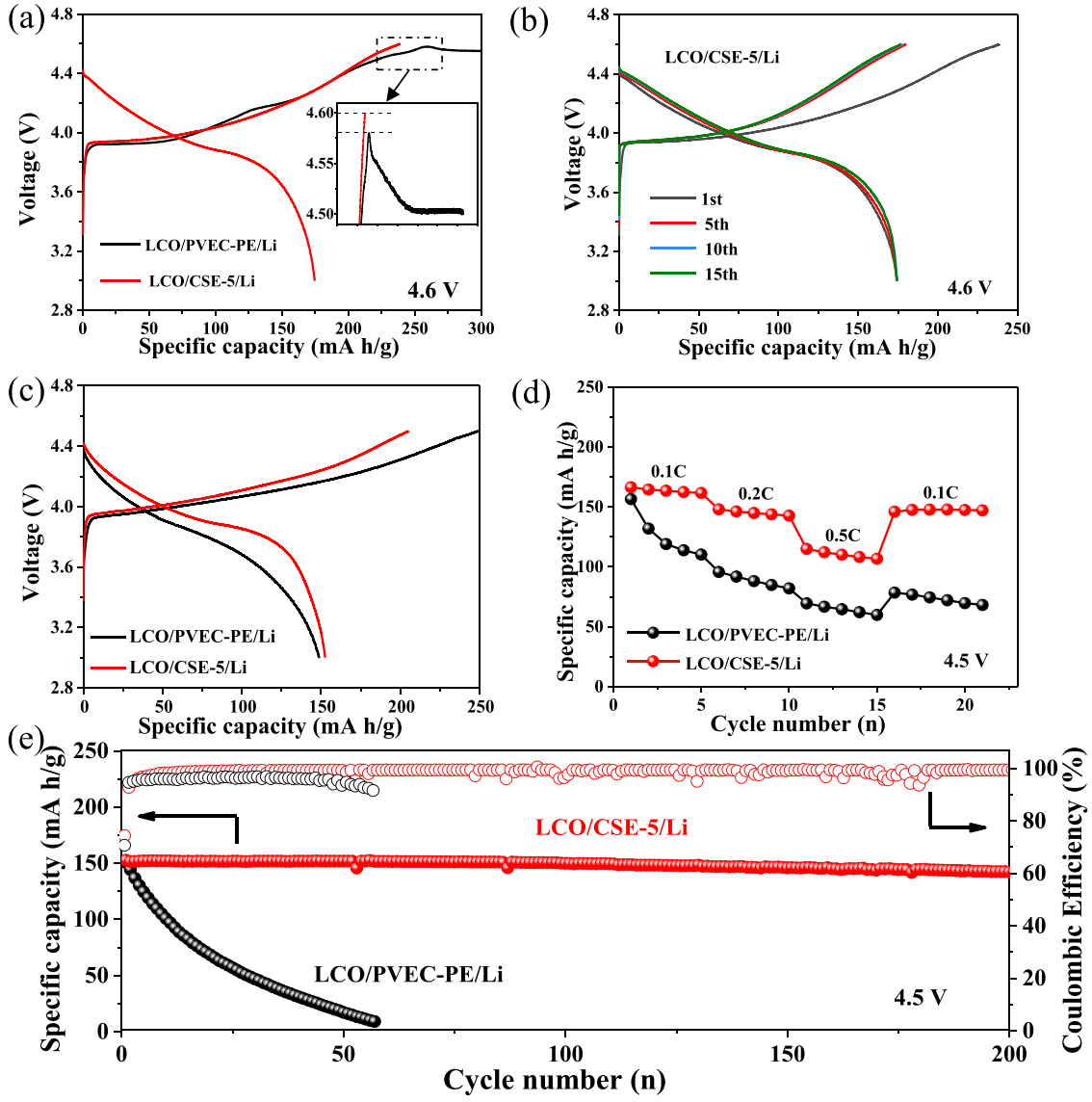

Fig. 5. (a) The initial charge/discharge curves of LCO/CSE-5/Li and LCO/PVEC-PE/Li batteries in the range of 3.0–4.6 V at 0.1 C. (b) The selected charge/discharge curves of LCO/CSE-5/Li battery. The comparisons of electrochemical performances between LCO/CSE-5/Li and LCO/PVEC-PE/Li batteries in the range of 3.0–4.5 V, including the (c) Initial charge/discharge curves at 0.1 C, (d) Rate performances, and (e) Cycling stability and Coulombic efficiency at 0.1 C.

5/Li battery should be attributed to the high t_{Li}^{+} with uniform distribution of ion concentration, which can reduce the side reaction between electrolyte and electrodes, and decrease the polarization of battery. Furthermore, the rate performances of solid-state batteries have been compared with the current densities increase from 0.1 C to 0.5 C (Fig. 5d). The LCO/CSE-5/Li battery exhibits the specific capacity of ~114 mA h/g at 0.5 C, which is much higher than that of LCO/PVEC-PE/Li battery at the same current density. As the polarization effect, the capacity decreases with the increase of current densities, and the overpotentials of the battery also increase simultaneously (Fig. S9b). However, the discharge capacity of LCO/CSE-5/Li battery can recover to ~150 mA h/g when the current density returns to 0.1 C, indicating the enhanced interface compatibility between polymer electrolyte and high-voltage cathode materials.

The cycling stabilities of solid-state batteries have also been compared (Fig. 5e and S9c). The LCO/CSE-5/Li battery still keeps the high capacity retention of ~94% over 200 cycles. However, the discharge capacity of LCO/PVEC-PE/Li battery decays dramatically over 50 cycles, and the battery is no longer able to work. Furthermore, the cycling stabilities of SSLBs with LCO cathode materials that charged to 4.5 V have been compared in Table S2, in which all the batteries are evaluated at 25 °C. Obviously, the LCO/CSE-5/Li battery shows the best performances among the different SSEs based batteries. The outstanding cycling stability of LCO/CSE-5/Li battery should be attributed to the enhanced anti-oxidation ability of electrolyte and favorable interface compatibility between electrolyte and the electrodes. Moreover, the structure and morphology of LCO material after 200 cycles were analyzed. From the XRD patterns and SEM images, there is no obvious structure change and crack of the cathode particles after long cycles (Fig. S10). The stable structure of LCO cathode material is also beneficial for the long cycling stability of solid-state battery.

The solid-state LCO/CSE-5/Li battery was also tested at different temperature, including 40 °C and 5 °C (Fig. S11). The battery delivers a high discharge capacity of ~158 mA h/g at 40 °C, and even ~125 mA h/g at 5 °C. The relatively high capacity at low temperature should be originated from the high ionic conductivity of CSE, which shows the potential application in the wide temperature range. Moreover, the electrochemical energy storage of solid-state LCO/CSE-5/Li battery has been explored by the pouch cell. Impressively, the cell can light up 70 light-emitting diode (LED) lamps that made the logo of "*BJUT*" (Fig. S12a). In particular, the pouch cell can still operate normally without short circuit or starting fire after cutting-off (Fig. S12b). Therefore, this CSE with wide electrochemical stability window and high ionic conductivity can be successfully applied for the high-voltage cathode materials, then the solid-state batteries offer high energy density and favorable electrochemical performances.

4. Conclusions

In summary, the composite solid electrolyte with wide electrochemical stability window up to ~5.0 V and high ionic conductivity of $\sim 1.35 \times 10^{-3}$ S/cm at 25 °C has been reported by the integration of SiO_2 nanoparticles and PVEC-PE. The enhanced anti-oxidation ability of polymer electrolyte was mainly caused by the local intermolecular interactions of hydrogen bonds that formed among components in composite electrolyte, and has been confirmed by theoretical calculations and experimental results. The composite electrolyte can be applied for high-voltage $LiCoO_2$ cathode material with charge potential of 4.5 V, and the corresponding solid-state battery shows the high capacity retention of ~94% after 200 cycles at 25 °C. Therefore, this study has not only proved the importance of intermolecular interactions for wide electrochemical stability window, but also provided the effective strategy to enhance the interface compatibility between polymer electrolyte and high-voltage cathodes for high-energy SSLBs.

CRediT authorship contribution statement

Haijun Yu and Khali Amine: Supervision, Writing – original draft, Formal analysis. **Yongtao Wang, Lingqiao Wu and Xianwei Guo**: Formal analysis, Writing – original draft. **Zhiyuan Lin and Peipei Ding**: Analyzing the experimental results. **Mingxue Tang**: SsNMR measurements. **Zihe Zhang**: Computational simulation. **Shiqi Liu and Boya Wang**: Raman and SEM measurements. **Xin Yin and Zonghai Chen**: Formal analysis and scientific discussion. [1]These authors contributed equally.

Declaration of Competing Interest

The authors declare that they have no known competing financial interests or personal relationships that could have appeared to influence the work reported in this paper.

Acknowledgements

This work was financially supported by "The Youth Beijing Scholars Program" (PXM2021_014204_000023), Beijing Natural Science Foundation (JQ19003), National Natural Science Foundation of China (Grants 21875007, 21975006, 21974007, and U19A2018) and Beijing Natural Science Foundation (KZ201910005002, KZ202010005007, and L182009), General Program of Science and Technology Development Project of Beijing Municipal Education Commission (KM202110005009), High-Grade Discipline Construction of Beijing (PXM2019-014204-500031) and China Postdoctoral Science Foundation (2021M700297). Research at Argonne National Laboratory was funded by the US Department of Energy (DOE), USA Vehicle Technologies Office. Support from Tien Duong of DOE's Vehicle Technologies Office is gratefully acknowledged. K.A. and H.J.Y acknowledge the support of the U.S. China Clean Energy Research Center (CERC-CVC2).

Appendix A. Supporting information

Supplementary data associated with this article can be found in the online version at doi:10.1016/j.nanoen.2022.107105.

References

[1] J.B. Goodenough, How we made the li-ion rechargeable battery, Nat. Electron. 1 (2018) 204, https://doi.org/10.1038/s41928-018-0048-6.
[2] M. Li, C. Wang, Z. Chen, K. Xu, J. Lu, New concepts in electrolytes, Chem. Rev. 120 (2020) 6783–6819, https://doi.org/10.1021/acs.chemrev.9b00531.
[3] H. Li, Practical evaluation of Li-ion batteries, Joule 3 (2019) 911–914, https://doi.org/10.1016/j.joule.2019.03.028.
[4] X. Zhang, B. Wang, S. Zhao, H. Li, H. Yu, Oxygen anionic redox activated high-energy cathodes: status and prospects, eTransportation 8 (2021), 100118, https://doi.org/10.1016/j.etran.2021.100118.
[5] X. Zhang, H. Yu, Crystalline domain battery materials, Acc. Chem. Res. 53 (2020) 368–379, https://doi.org/10.1021/acs.accounts.9b00457.
[6] S. Liu, B. Wang, X. Zhang, S. Zhao, Z. Zhang, H. Yu, Reviving the lithium-manganese-based layered oxide cathodes for lithium-ion batteries, Matter 4 (2021) 1511–1527, https://doi.org/10.1016/j.matt.2021.02.023.
[7] Y. Wang, E. Wang, X. Zhang, H. Yu, High-voltage "single-crystal" cathode materials for lithium-ion batteries, Energy Fuels 35 (2021) 1918–1932, https://doi.org/10.1021/acs.energyfuels.0c03608.
[8] Z. Gao, H. Sun, L. Fu, F. Ye, Y. Zhang, W. Luo, Y. Huang, Promises, challenges, and recent progress of inorganic solid-state electrolytes for all-solid-state lithium batteries, Adv. Mater. 30 (2018), 1705702, https://doi.org/10.1002/adma.201705702.
[9] C. Wang, K. Fu, S.P. Kammampata, D.W. McOwen, A.J. Samson, L. Zhang, G. T. Hitz, A.M. Nolan, E.D. Wachsman, Y. Mo, V. Thangadurai, L. Hu, Garnet-type solid-state electrolytes: materials, interfaces, and batteries, Chem. Rev. 120 (2020) 4257–4300, https://doi.org/10.1021/acs.chemrev.9b00427.
[10] L. Fan, S. Wei, S. Li, Q. Li, Y. Lu, Recent progress of the solid-state electrolytes for high-energy metal-based batteries, Adv. Energy Mater. 8 (2018), 1702657, https://doi.org/10.1002/aenm.201702657.
[11] N. Zhao, W. Khokhar, Z. Bi, C. Shi, X. Guo, L.-Z. Fan, C.-W. Nan, Solid garnet batteries, Joule 3 (2019) 1190–1199, https://doi.org/10.1016/j.joule.2019.03.019.

[12] J.C. Bachman, S. Muy, A. Grimaud, H.H. Chang, N. Pour, S.F. Lux, O. Paschos, F. Maglia, S. Lupart, P. Lamp, L. Giordano, Y. Shao-Horn, Inorganic solid-state electrolytes for lithium batteries: mechanisms and properties governing ion conduction, Chem. Rev. 116 (2016) 140–162, https://doi.org/10.1021/acs.chemrev.5b00563.

[13] R. Chen, W. Qu, X. Guo, L. Li, F. Wu, The pursuit of solid-state electrolytes for lithium batteries: from comprehensive insight to emerging horizons, Mater. Horiz. 3 (2016) 487–516, https://doi.org/10.1039/c6mh00218h.

[14] D. Zhou, D. Shanmukaraj, A. Tkacheva, M. Armand, G. Wang, Polymer electrolytes for lithium-based batteries: advances and prospects, Chem 5 (2019) 2326–2352, https://doi.org/10.1016/j.chempr.2019.05.009.

[15] J. Zhang, J. Zhao, L. Yue, Q. Wang, J. Chai, Z. Liu, X. Zhou, H. Li, Y. Guo, G. Cui, L. Chen, Safety-reinforced poly(propylene carbonate)-based all-solid-state polymer electrolyte for ambient-temperature solid polymer lithium batteries, Adv. Energy Mater. 5 (2015), 1501082, https://doi.org/10.1002/aenm.201501082.

[16] P. Wang, J. Chai, Z. Zhang, H. Zhang, Y. Ma, G. Xu, H. Du, T. Liu, G. Li, G. Cui, An iintricately designed poly(vinylene carbonate-acrylonitrile) copolymer electrolyte enables 5 V lithium batteries, J. Mater. Chem. A 7 (2019) 5295–5304, https://doi.org/10.1039/c9ta00204a.

[17] C.V. Amanchukwu, Z. Yu, X. Kong, J. Qin, Y. Cui, Z. Bao, A new class of ionically conducting fluorinated ether electrolytes with high electrochemical stability, J. Am. Chem. Soc. 142 (2020) 7393–7403, https://doi.org/10.1021/jacs.9b11056.

[18] J. Li, Y. Lin, H. Yao, C. Yuan, J. Liu, Tuning thin-film electrolyte for lithium battery by grafting cyclic carbonate and combed poly(ethylene oxide) on polysiloxane, ChemSusChem 7 (2014) 1901–1908, https://doi.org/10.1002/cssc.201400113.

[19] R. Bouchet, S. Maria, R. Meziane, A. Aboulaich, L. Lienafa, J.-P. Bonnet, T.N. T. Phan, D. Bertin, D. Gigmes, D. Devaux, R. Denoyel, M. Armand, Single-ion BAB triblock copolymers as highly efficient electrolytes for lithium-metal batteries, Nat. Mater. 12 (2013) 452–457, https://doi.org/10.1038/namt3602.

[20] J. Liu, X. Shen, J. Zhou, M. Wang, C. Niu, T. Qian, C. Yan, Nonflammable and high-voltage-tolerated polymer electrolyte achieving high stability and safety in 4.9 V-class lithium metal battery, ACS Appl. Mater. Interfaces 11 (2019) 45048–45056, https://doi.org/10.1021/acsami.9b14147.

[21] Z. Lin, X. Guo, Z. Wang, B. Wang, S. He, L.A. O'Dell, J. Huang, H. Li, H. Yu, L. Chen, A wide-temperature superior ionic conductive polymer eectrolyte for lithium metal battery, Nano Energy 73 (2020), 104786, https://doi.org/10.1016/j.nanoen.2020.104786.

[22] P. Fan, H. Liu, V. Marosz, N.T. Samuels, S.L. Suib, L. Sun, L. Liao, High performance composite polymer electrolytes for lithium-ion batteries, Adv. Funct. Mater. 31 (2021), 2101380, https://doi.org/10.1002/adfm.202101380.

[23] B. Xu, X. Li, C. Yang, Y. Li, N.S. Grundish, P.-H. Chien, K. Dong, I. Manke, R. Fang, N. Wu, H. Xu, A. Dolocan, J.B. Goodenough, Interfacial chemistry enables stable cycling of all-solid-state Li metal batteries at high current densities, J. Am. Chem. Soc. 143 (2021) 6542–6550, https://doi.org/10.1021/jacs.1c00752.

[24] W. Liu, D. Lin, J. Sun, G. Zhou, Y. Cui, Improved lithium ionic conductivity in composite polymer electrolytes with oxide-ion conducting nanowires, ACS Nano 10 (2016) 11407–11413, https://doi.org/10.1021/acsnano.6b06797.

[25] T. Jiang, P. He, G. Wang, Y. Shen, C.W. Nan, L.Z. Fan, Solvent-free synthesis of thin, flexible, nonflammable garnet-based composite solid electrolyte for all-solidstate lithium batteries, Adv. Energy Mater. 10 (2020), 1903376, https://doi.org/10.1002/aenm.201903376.

[26] H. Huo, Y. Chen, J. Luo, X. Yang, X. Guo, X. Sun, Rational design of hierarchical "ceramic-in-polymer" and "polymer-in-ceramic" electrolytes for dendrite-free solid-state batteries, Adv. Energy Mater. 9 (2019), 1804004, https://doi.org/10.1002/aenm.201804004.

[27] K.K. Fu, Y. Gong, J. Dai, A. Gong, X. Han, Y. Yao, C. Wang, Y. Wang, Y. Chen, C. Yan, Y. Li, E.D. Wachsman, L. Hu, Flexible, solid-state, ion-conducting membrane with 3D garnet nanofiber networks for lithium batteries, Proc. Natl. Acad. Sci. USA 113 (2016) 7094–7099.

[28] X. Zhang, T. Liu, S. Zhang, X. Huang, B. Xu, Y. Lin, B. Xu, L. Li, C.W. Nan, Y. Shen, Synergistic coupling between $Li_{6.75}La_3Zr_{1.75}Ta_{0.25}O_{12}$ and poly(vinylidene fluoride) induces high ionic conductivity, mechanical strength, and thermal stability of solid composite electrolytes, J. Am. Chem. Soc. 139 (2017) 13779–13785, https://doi.org/10.1021/jacs.7b06364.

[29] W. Chen, J. Shi, Y. Qian, J. Wan, X. Zhang, H. Sheng, B. Guan, R. Wen, Y. Yin, S. Xin, Y. Guo, L. Wan, Bridging interparticle Li^+ conduction in a soft ceramic oxide, J. Am. Chem. Soc. 143 (2021) 5717–5726, https://doi.org/10.1021/jacs.0c12965.

[30] H. Duan, M. Fan, W. Chen, J.Y. Li, P. Wang, W. Wang, J. Shi, Y. Yin, L. Wan, Y. Guo, Extended electrochemical window of solid electrolytes via heterogeneous multilayered structure for high-voltage lithium metal batteries, Adv. Mater. 31 (2019), e1807789, https://doi.org/10.1002/adma.201807789.

[31] K. Pan, L. Zhang, W. Qian, X. Wu, K. Dong, H. Zhang, S. Zhang, A flexible ceramic/polymer hybrid solid electrolyte for solid-state lithium metal batteries, Adv. Mater. 32 (2020), e2000399, https://doi.org/10.1002/adma.202000399.

[32] C. Park, Electrochemical stability and conductivity enhancement of composite polymer electrolytes, Solid State Ion. 159 (2003) 111–119, https://doi.org/10.1016/s0167-2738(03)00025-0.

[33] H. Chen, D. Adekoya, L. Hencz, J. Ma, S. Chen, C. Yan, H. Zhao, G. Cui, S. Zhang, Stable seamless interfaces and rapid ionic conductivity of Ca–CeO_2 /LiTFSI/PEO composite electrolyte for high-rate and high-voltage all-solid-state battery, Adv. Energy Mater. 10 (2020), 2000049, https://doi.org/10.1002/aenm.202000049.

[34] N. Wu, P.H. Chien, Y. Li, A. Dolocan, H. Xu, B. Xu, N.S. Grundish, H. Jin, Y.Y. Hu, J. B. Goodenough, Fast $Li^{(+)}$ conduction mechanism and interfacial chemistry of a NASICON/polymer composite electrolyte, J. Am. Chem. Soc. 142 (2020) 2497–2505, https://doi.org/10.1021/jacs.9b12233.

[35] M.J. Frisch, G.W. Trucks, H.B. Schlegel, G.E. Scuseria, M.A. Robb, J.R. Cheeseman, G. Scalmani, V. Barone, B. Mennucci, G.A. Petersson, Gaussian 09, Gaussian Inc., Wallingford, CT, 2009.

[36] B. A.D, Density-functional thermochemistry. III. The role of exact exchange, J. Chem. Phys. (1993) 5648–5652.

[37] P.J. Stephens, F.J. Devlin, C.F. Chabalowski, M.J. Frisch, Ab initio calculation of vibrational absorption and circular dichroism spectra using density functional force fields, J. Phys. Chem. 98 (1994) 11623–11627.

[38] S. Grimme, J. Antony, S. Ehrlich, H. Krieg, A consistent and accurate ab initio parametrization of density functional dispersion correction (DFT-D) for the 94 Elements H-Pu, J. Chem. Phys. 132 (2010), 154104, https://doi.org/10.1063/1.3382344.

[39] S. Grimme, S. Ehrlich, L. Goerigk, Effect of the damping function in dispersion corrected density functional theory, J. Comput. Chem. 32 (2011) 1456–1465, https://doi.org/10.1002/jcc.21759.

[40] R. Sarkar, T.K. Kundu, Density functional theory studies on PVDF/Ionic liquid composite systems, J. Chem. Sci. 130 (2018) 115, https://doi.org/10.1007/s12039-018-1522-4.

[41] L. Liu, L. Miao, L. Li, F. Li, Y. Lu, Z. Shang, J. Chen, Molecular electrostatic potential: a new tool to predict the lithiation process of organic battery materials, J. Phys. Chem. Lett. 9 (2018) 3573–3579, https://doi.org/10.1021/acs.jpclett.8b01123.

[42] L. Miao, L. Liu, K. Zhang, J. Chen, Molecular design strategy for high-redox-potential and poorly soluble n-type phenazine derivatives as cathode materials for lithium batteries, ChemSusChem 13 (2020) 2337–2344, https://doi.org/10.1002/cssc.202000004.

[43] A. Bakker, S. Gejji, J. Lindgren, K. Hermansson, M.M. Probst, Polymer-contact ion pair formation and ether oxygen coordination in the polymer electrolytes M[N(CF3SO2)2]2PEOn for M = Mg, Ca, Sr and Ba. Polymer 36 (1995) 4371–4378, https://doi.org/10.1016/0032-3861(95)96841-U.

[44] Z. Wang, W. Gao, X. Huang, Y. Mo, L. Chen, Spectroscopic studies on interactions and microstructures in propylene carbonate LiTFSI electrolytes, J. Raman Spectrosc. 32 (2001) 900–905, https://doi.org/10.1002/jrs.756.

[45] J.-C. Lassègues, J. Grondin, C. Aupetit, P. Johansson, Spectroscopic identification of the lithium ion transporting species in LiTFSI-doped ionic liquids, J. Phys. Chem. A 113 (2009) 305–314.

[46] K. Wen, X. Tan, T. Chen, S. Chen, S. Zhang, Fast Li-ion transport and uniform Li-ion flux enabled by a double–layered polymer electrolyte for high performance Li metal battery, Energy Stor. Mater. 32 (2020) 55–64, https://doi.org/10.1016/j.ensm.2020.07.037.

[47] Y. Kuai, F. Wang, J. Yang, H. Lu, Z. Xu, X. Xu, Y. NuLi, J. Wang, Silica-nanoresin crosslinked composite polymer electrolyte for ambient-temperature all-solid-state lithium batteries, Mater. Chem. Front. 5 (2021) 6502–6511, https://doi.org/10.1039/d1qm00769f.

[48] S.L. Warring, D.A. Beattie, A.J. McQuillan, Surficial siloxane-to-silanol interconversion during room-temperature hydration/dehydration of amorphous silica films observed by ATR-IR and TIR-raman spectroscopy, Langmuir 32 (2016) 1568–1576, https://doi.org/10.1021/acs.langmuir.5b04506.

[49] N. Cioica, R. Fechete, C. Cota, E.M. Nagy, L. David, O. Cozar, NMR relaxation investigation of the native corn starch structure with plasticizers, J. Mol. Struct. 1044 (2013) 128–133, https://doi.org/10.1016/j.molstruc.2013.01.037.

[50] H. Zhu, H.P. Huinink, P.C. Magusin, O.C. Adan, K. Kopinga, T(2) distribution spectra obtained by continuum fitting method using a mixed Gaussian and exponential kernel function, J. Magn. Reson 235 (2013) 109–114, https://doi.org/10.1016/j.jmr.2013.08.002.

[51] S. Li, Y.-M. Chen, W. Liang, Y. Shao, K. Liu, Z. Nikolov, Y. Zhu, A superionic conductive, electrochemically stable dual-salt polymer electrolyte, Joule 2 (2018) 1838–1856, https://doi.org/10.1016/j.joule.2018.06.008.

[52] Y. Zhu, F. Wang, L. Liu, S. Xiao, Z. Chang, Y. Wu, Composite of A nonwoven fabric with poly(vinylidene fluoride) as A gel membrane of high safety for lithium ion battery, Energy Environ. Sci. 6 (2013) 618–624, https://doi.org/10.1039/c2ee23564a.

[53] J. Chai, Z. Liu, J. Ma, J. Wang, X. Liu, H. Liu, J. Zhang, G. Cui, L. Chen, In SItu Generation of Poly (Vinylene Carbonate) based solid electrolyte with interfacial stability for $LiCoO_2$ lithium batteries, Adv. Sci. 4 (2017), 1600377, https://doi.org/10.1002/advs.201600377.

[54] M. Armand, Polymer SOlid Electrolytes - an Overview, Solid State Ion. 9 (1983) 745–754.

[55] S. Ko, Y. Yamada, A. Yamada, An overlooked issue for high-voltage li-ion batteries: suppressing the intercalation of anions into conductive carbon, Joule 5 (2021) 998–1009, https://doi.org/10.1016/j.joule.2021.02.016.

[56] Y. He, B. Zhu, Y. Inoue, Hydrogen bonds in polymer blends, Prog. Polym. Sci. 29 (2004) 1021–1051, https://doi.org/10.1016/j.progpolymsci.2004.07.002.

[57] M.M. Coleman, P.C. Painter, Hydrogen bonded polymer blends, Prog. Polym. Sci. 20 (1995) 1–59.

[58] G. Liu, J. Xie, S. Wang, Q. Wang, S. Gao, Y. Yuan, J. Lu, Hydrogen-bonding reinforced flexible composite electrodes for enhanced energy storage, Adv. Funct. Mater. 32 (2021), 202108003, https://doi.org/10.1002/adfm.202108003.

[59] D. Lin, W. Liu, Y. Liu, H.R. Lee, P.C. Hsu, K. Liu, Y. Cui, High ionic conductivity of composite solid polymer electrolyte via in situ synthesis of monodispersed SiO2 nanospheres in poly(ethylene oxide), Nano Lett. 16 (2016) 459–465, https://doi.org/10.1021/acs.nanolett.5b04117.

[60] N. Wu, P.H. Chien, Y. Qian, Y. Li, H. Xu, N.S. Grundish, B. Xu, H. Jin, Y.Y. Hu, G. Yu, J.B. Goodenough, Enhanced surface interactions enable Fast $Li^{(+)}$ conduction in oxide/polymer composite electrolyte, Angew. Chem. Int. Ed. Engl. 59 (2020) 4131–4137, https://doi.org/10.1002/anie.201914478.

[61] J. Zheng, M. Tang, Y.Y. Hu, Lithium ion pathway within $Li_7La_3Zr_2O_{12}$ -polyethylene oxide composite electrolytes, Angew. Chem. Int. Ed. Engl. 55 (2016) 12538–12542, https://doi.org/10.1002/anie.201607539.
[62] J. Zheng, Y.Y. Hu, New insights into the compositional dependence of Li-Ion transport in polymer-ceramic composite electrolytes, ACS Appl. Mater. Interfaces 10 (2018) 4113–4120, https://doi.org/10.1021/acsami.7b17301.
[63] C. Hu, Y. Shen, M. Shen, X. Liu, H. Chen, C. Liu, T. Kang, F. Jin, L. Li, J. Li, Y. Li, N. Zhao, X. Guo, W. Lu, B. Hu, L. Chen, Superionic conductors via bulk interfacial conduction, J. Am. Chem. Soc. 142 (2020) 18035–18041, https://doi.org/10.1021/jacs.0c07060.
[64] Z. Li, H.M. Huang, J.K. Zhu, J.F. Wu, H. Yang, L. Wei, X. Guo, Ionic conduction in composite polymer electrolytes: case of PEO:Ga-LLZO composites, ACS Appl. Mater. Interfaces 11 (2019) 784–791, https://doi.org/10.1021/acsami.8b17279.
[65] J. Qiu, X. Liu, R. Chen, Q. Li, Y. Wang, P. Chen, L. Gan, S.-J. Lee, D. Nordlund, Y. Liu, X. Yu, X. Bai, H. Li, L. Chen, Enabling stable cycling of 4.2 V high-voltage allsolid- state batteries with PEO-based solid electrolyte, Adv. Funct. Mater. 30 (2020), 1909392, https://doi.org/10.1002/adfm.201909.
[66] Q. Yang, J. Huang, Y. Li, Y. Wang, J. Qiu, J. Zhang, H. Yu, X. Yu, H. Li, L. Chen, Surface-protected $LiCoO_2$ with ultrathin solid oxide electrolyte film for high-voltage lithium ion batteries and lithium polymer batteries, J. Power Sources 388 (2018) 65–70, https://doi.org/10.1016/j.jpowsour.2018.03.076.
[67] J. Liang, Y. Sun, Y. Zhao, Q. Sun, J. Luo, F. Zhao, X. Lin, X. Li, R. Li, L. Zhang, S. Lu, H. Huang, X. Sun, Engineering the conductive carbon/PEO interface to stabilize solid polymer electrolytes for all-solid-state high voltage $LiCoO_2$ batteries, J. Mater. Chem. A 8 (2020) 2769–2776, https://doi.org/10.1039/c9ta08607b.